

Refinement of the magnetic composite model of type 304 stainless steel by considering misoriented ferromagnetic martensite particles

Katsuyuki Kinoshita

Citation: *AIP Advances* **7**, 056008 (2017); doi: 10.1063/1.4974068

View online: <http://dx.doi.org/10.1063/1.4974068>

View Table of Contents: <http://aip.scitation.org/toc/adv/7/5>

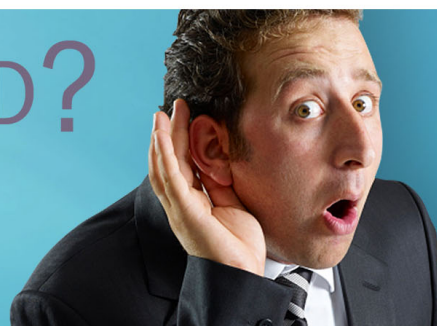
Published by the [American Institute of Physics](#)

HAVE YOU HEARD?

Employers hiring scientists and
engineers trust

PHYSICS TODAY | JOBS

www.physicstoday.org/jobs



Refinement of the magnetic composite model of type 304 stainless steel by considering misoriented ferromagnetic martensite particles

Katsuyuki Kinoshita^a

Department of Energy Conversion Science, Graduate School of Energy Science, Kyoto University, Yoshida-honmachi, Sakyo-ku, Kyoto 606-8501, Japan

(Presented 1 November 2016; received 23 September 2016; accepted 26 October 2016; published online 11 January 2017)

We improved a magnetic composite model that combines the Jiles–Atherton model and Eshelby’s equivalent inclusion method to consider misoriented martensite particles. The magnetic permeability of type 304 stainless steel were analyzed by using both experimental data on the orientation distribution of type 304 stainless steel specimens and the improved model. We found that the model is able to qualitatively explain the variation of permeability with the orientation angle and orientation distribution, an effect that depends on the direction of the excitation magnetic field. © 2017 Author(s). All article content, except where otherwise noted, is licensed under a Creative Commons Attribution (CC BY) license (<http://creativecommons.org/licenses/by/4.0/>). [<http://dx.doi.org/10.1063/1.4974068>]

I. INTRODUCTION

Type 304 stainless steel (SUS304 steel) is normally paramagnetic, but it is a unique material in which plastic deformation induces a transformation to the ferromagnetic martensite phase. This characteristic has been used to assess fatigue degradation¹ and the extent of plastic deformation.² However, for this, it is important to develop a magnetic composite model that allows us to predict the magnetic properties of SUS304 steel. Magnetic composite models using an effective medium approach^{3,4} have been developed to characterize dynamic magnetic behavior such as ferromagnetic resonance. As an alternative approach, a magnetic composite model using Eshelby’s equivalent inclusion method⁵ was introduced to describe the behavior of magnetoelastic composite materials.⁶ The latter has the advantage that it allows for coupled analysis. However, to our knowledge, a magnetic composite model to describe static magnetic properties, such as the hysteresis loop, has not been developed yet.

In a previous work, we derived a magnetic composite model⁷ that combined Eshelby’s equivalent inclusion method and the Jiles–Atherton model (J–A model).⁸ However, that derived model did not incorporate the orientation angle and orientation distribution of the martensite phase. In this study, we derived a magnetic composite model that allows for misoriented martensite particles, and investigated the influence of these particles on the permeability in SUS304 steel.

II. MATHEMATICAL MODEL

As shown in Fig. 1(a), needle-type particles (martensite particles, MPs) are generated in a grain of SUS304 steel as a ferromagnetic martensite phase, and those grains are distributed in a test piece. Therefore, we need to consider two different interactions: those between the MPs in a grain and those between groups of MPs. MPs in a grain are modeled as single ellipsoidal inhomogeneity (equivalent martensite particle, EMP) whose nonlinear magnetic behavior is described by the J–A model. In this

^aElectronic mail: kinosita@energy.kyoto-u.ac.jp

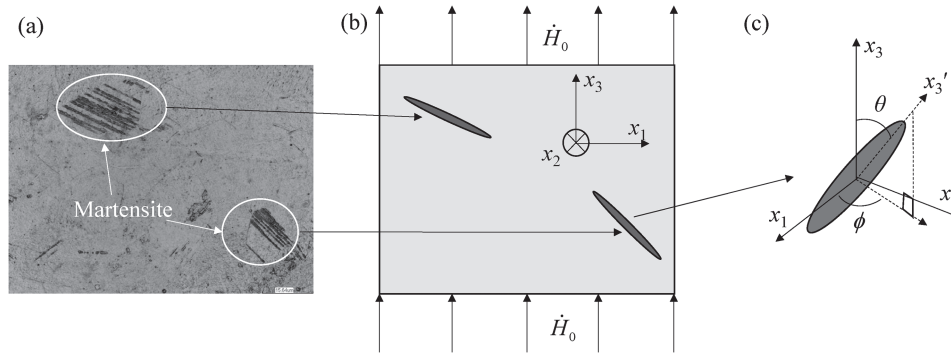


FIG. 1. Schematic of the modeling of a magnetic composite; (a) Laser micrograph of SUS304 steel, (b) boundary condition, and (c) coordinate system.

study, the EMPs are assumed to be prolate spheroid. The interaction between the MPs is accounted for by the interaction term α of the J-A model. Based on that model, the differential magnetic susceptibility χ_f of an EMP can be written as

$$\chi_f = \left\{ k\delta c \frac{dM_f^{an}}{dH_f^e} + \delta_M (M_f^{an} - M_f) \right\} / \left[k\delta - \alpha \left\{ k\delta c \frac{dM_f^{an}}{dH_f^e} + \delta_M (M_f^{an} - M_f) \right\} \right], \quad (1)$$

where α , k , and c are model parameters, the subscript f represents the martensite phase, H^e is the effective magnetic field, M^{an} is the anhysteretic magnetization (described by the Langevin function), δ denotes the sign of dH_f/dt , and $\delta_M = 0.5[1 + \text{sign}((M_f^{an} - M_f)\dot{H}_f)]$.

The magnetic behavior of the composite is described by incremental equations based on the Eshelby's equivalent inclusion method, and the interaction between the EMPs by using the Mori-Tanaka theory.⁹ The effect of the orientation distribution of the EMPs was introduced in the model using a method similar to those of Hatta et al.¹⁰ and Dunn et al.¹¹ Let the x_3 -axis point in the longitudinal direction of the test piece and the x_3' -axis coincide with the fiber axis, as shown in Fig. 1(c). The magnetic composite is subjected to a uniform incremental magnetic field \dot{H}_0 in the x_3 direction. The orientation of an EMP is defined by two angles θ and ϕ . Using Eshelby's equivalent inclusion method, an incremental magnetic flux in the EMP can be written in the local coordinate system through the following vector equation

$$\dot{B}_f' = \mu_f (\dot{H}_0' + \dot{\bar{H}}' + \dot{\tilde{H}}') = \mu_m (\dot{H}_0' + \dot{\bar{H}}' + \dot{\tilde{H}}' - \dot{H}^{*'}), \quad (2)$$

where μ is the differential permeability, $\dot{\bar{H}}'$ is the incremental average disturbance of the magnetic field (an interaction term), $\dot{\tilde{H}}'$ is the incremental magnetic field disturbed by the existence of the EMP, $\dot{H}^{*'}$ is the incremental eigen magnetic field, and the subscript m denotes the austenite phase. The incremental eigen magnetic field is defined using $\dot{\tilde{H}}'$ and the Eshelby's tensor¹⁰ S by Eq. (3).

$$\dot{\tilde{H}}' = S \dot{H}^{*'}. \quad (3)$$

Inserting Eq. (3) into Eq. (2) and rearranging the terms, we obtain

$$\dot{H}^{*' } = \{ (\mu_f - \mu_m)S + \mu_m \}^{-1} (\mu_m - \mu_f) (\dot{H}_0' + \dot{\bar{H}}'), \quad (4)$$

$$\dot{\tilde{H}}' = S \{ (\mu_f - \mu_m)S + \mu_m \}^{-1} (\mu_m - \mu_f) (\dot{H}_0' + \dot{\bar{H}}'). \quad (5)$$

Based on Fig. 1(c), a vector can be transformed between the global and local coordinates as follows:

$$\mathbf{y}' = X\mathbf{y}, \mathbf{y} = X^{-1}\mathbf{y}', \quad X = \begin{pmatrix} \cos \theta \cos \phi & \cos \theta \sin \phi & -\sin \theta \\ -\sin \phi & \cos \phi & 0 \\ \sin \theta \cos \phi & \sin \theta \sin \phi & \cos \theta \end{pmatrix}. \quad (6)$$

Using Eq. (6) to write Eqs. (4) and (5) in global coordinates, we obtain

$$\dot{\mathbf{H}}^* = \mathbf{X}^{-1} \{(\boldsymbol{\mu}_f - \boldsymbol{\mu}_m)\mathbf{S} + \boldsymbol{\mu}_m\}^{-1} (\boldsymbol{\mu}_m - \boldsymbol{\mu}_f)\mathbf{X}(\dot{\mathbf{H}}_0 + \dot{\tilde{\mathbf{H}}}) = \mathbf{M}(\dot{\mathbf{H}}_0 + \dot{\tilde{\mathbf{H}}}), \quad (7)$$

$$\dot{\tilde{\mathbf{H}}} = \mathbf{X}^{-1}\mathbf{S} \{(\boldsymbol{\mu}_f - \boldsymbol{\mu}_m)\mathbf{S} + \boldsymbol{\mu}_m\}^{-1} (\boldsymbol{\mu}_m - \boldsymbol{\mu}_f)\mathbf{X}(\dot{\mathbf{H}}_0 + \dot{\tilde{\mathbf{H}}}) = \mathbf{N}(\dot{\mathbf{H}}_0 + \dot{\tilde{\mathbf{H}}}). \quad (8)$$

When the EMP orientation angles are within the ranges $\theta_a \leq \theta \leq \theta_b$ and $\phi_a \leq \phi \leq \phi_b$, the volume average of $\dot{\mathbf{H}}^{*'}$ and $\dot{\tilde{\mathbf{H}}}'$ over the entire composite can be obtained by discrete integration:

$$\langle \dot{\mathbf{H}}^* \rangle = \sum_{\theta=\theta_a}^{\theta_b} \sum_{\phi=\phi_a}^{\phi_b} g(\theta, \phi) \sin \theta \dot{\mathbf{H}}^* \Delta\theta \Delta\phi = \sum_{\theta=\theta_a}^{\theta_b} \sum_{\phi=\phi_a}^{\phi_b} g(\theta, \phi) \sin \theta \mathbf{M} \Delta\theta \Delta\phi (\dot{\mathbf{H}}_0 + \dot{\tilde{\mathbf{H}}}) = \mathbf{Q}^* (\dot{\mathbf{H}}_0 + \dot{\tilde{\mathbf{H}}}), \quad (9)$$

$$\langle \dot{\tilde{\mathbf{H}}} \rangle = \sum_{\theta=\theta_a}^{\theta_b} \sum_{\phi=\phi_a}^{\phi_b} g(\theta, \phi) \sin \theta \dot{\tilde{\mathbf{H}}} \Delta\theta \Delta\phi = \sum_{\theta=\theta_a}^{\theta_b} \sum_{\phi=\phi_a}^{\phi_b} g(\theta, \phi) \sin \theta \mathbf{N} \Delta\theta \Delta\phi (\dot{\mathbf{H}}_0 + \dot{\tilde{\mathbf{H}}}) = \tilde{\mathbf{Q}} (\dot{\mathbf{H}}_0 + \dot{\tilde{\mathbf{H}}}), \quad (10)$$

where $g(\theta, \phi)$ is a probability density function, and $\langle \rangle$ denotes volume average. When the magnetic composite is subjected to an applied magnetic field, as shown in Fig. 1(b), the relationship between the interaction field $\dot{\tilde{\mathbf{H}}}$ and $\langle \dot{\tilde{\mathbf{H}}} \rangle$ is given by¹¹

$$\dot{\tilde{\mathbf{H}}} = -V_f \langle \dot{\tilde{\mathbf{H}}} \rangle, \quad (11)$$

where V_f is the martensite fraction. The relationship between the incremental magnetic flux density and the incremental magnetic field can be found by using the law-of-mixtures formula¹² for the incremental magnetic flux density, together with Eqs. (2) and (11):

$$\langle \dot{\mathbf{B}}_c \rangle = \boldsymbol{\mu}_m (\dot{\mathbf{H}}_0 - V_f \langle \dot{\mathbf{H}}^* \rangle) = \boldsymbol{\mu}_m \left\{ \mathbf{I} - V_f \mathbf{Q}^* + V_f^2 \mathbf{Q}^* (\mathbf{I} + V_f \tilde{\mathbf{Q}})^{-1} \tilde{\mathbf{Q}} \right\} \dot{\mathbf{H}}_0, \quad (12)$$

where c denotes the magnetic composite and \mathbf{I} is the unit matrix. The internal magnetic field of the EMP in the local coordinates, needed to calculate Eq. (1), is given as

$$\dot{\mathbf{H}}_f' = \dot{\mathbf{H}}_0' + \dot{\tilde{\mathbf{H}}}' + \dot{\tilde{\mathbf{H}}}' = \left[\mathbf{I} + \mathbf{S} \{(\boldsymbol{\mu}_f - \boldsymbol{\mu}_m)\mathbf{S} + \boldsymbol{\mu}_m\}^{-1} (\boldsymbol{\mu}_m - \boldsymbol{\mu}_f) \right] \mathbf{X} \left\{ \mathbf{I} - V_f (\mathbf{I} + V_f \tilde{\mathbf{Q}})^{-1} \tilde{\mathbf{Q}} \right\} \dot{\mathbf{H}}_0. \quad (13)$$

For the probability density function appearing in Eqs. (9) and (10), we use the form proposed by Maekawa et al.¹³ to express the fiber orientation distribution in a fiber-reinforced composite. The following equation describes the three-dimensional orientation distribution with n peaks.

$$g(\theta, \phi) = g_i(\theta, \phi) = \frac{\left\{ \sin \left(\frac{\theta}{2} \right) \right\}^{2P_i-1} \left\{ \cos \left(\frac{\theta}{2} \right) \right\}^{2Q_i-1}}{\sum_{j=1}^n \alpha_j} \times \frac{\left\{ \sin \left(\frac{\phi}{2} \right) \right\}^{2R_i-1} \left\{ \cos \left(\frac{\phi}{2} \right) \right\}^{2S_i-1}}{\sum_{j=1}^n \beta_j}, \quad (14)$$

where P_i, Q_i, R_i and S_i are parameters of the material,

$$\alpha_j = \int_{\theta_j}^{\theta_{j+1}} \left\{ \sin \left(\frac{\theta}{2} \right) \right\}^{2P_j-1} \left\{ \cos \left(\frac{\theta}{2} \right) \right\}^{2Q_j-1} d\theta, \quad \beta_j = \int_{\phi_j}^{\phi_{j+1}} 2 \left\{ \sin \left(\frac{\phi}{2} \right) \right\}^{2R_j} \left\{ \cos \left(\frac{\phi}{2} \right) \right\}^{2S_j} d\phi, ,$$

and $\theta_i \leq \theta < \theta_{i+1}$, $\phi_i \leq \phi < \phi_{i+1}$, ($i = 1, \dots, n$).

III. EXPERIMENTAL METHOD

The test specimens used were cold-rolled plates of SUS304 steel (2B finish) with a gage length of 60 mm, a width of 12.5 mm, and a thickness of 2 mm. Maximum nominal strains of approximately 0.05, 0.1, 0.2, 0.3, and 0.4 were applied to them using a tensile machine and non-contact video extensometer to generate different martensite phases. Aspect ratios (major axis length/minor axis

length) and orientation angles of the MPs in the test pieces were measured using image processing software, after first polishing the surface by buffing and then chemical etching.¹⁴ A magnetic field with triangular wave form was set up along the longitudinal direction of the specimens using an electromagnet, and the magnetic flux density was measured by means of a search coil. Permeability was estimated through a differential permeability curve, obtained from the magnetic flux density curve and the evaluation parameter

$$\psi = \left| \int_0^{H^{\max}} \{\mu(H) - \mu(0)\} / \mu(0) dH \right|. \quad (15)$$

IV. RESULTS AND DISCUSSION

Figure 2 shows histograms of the measured orientation distribution of the MPs for each specimen together with the best-fit curve calculated from Eq. (14). As it was difficult to measure the three-dimensional orientation distribution of the MP, we evaluated the two-dimensional orientation distribution for $\phi = 0$ and $n = 2$. Because it was difficult to etch uniformly on the entire surface of the specimen, the number of data points was not sufficient to produce a histogram. Therefore, we assumed that the orientation distribution in the range $0^\circ \leq \theta < 90^\circ$ was the same as that in $90^\circ \leq \theta < 180^\circ$, and then estimated the parameters P_1 and S_1 of the probability density function as $P_1 = P_2$, $S_1 = S_2$. Moreover, J–A parameters were calculated from the magnetization curve for SUS410S (martensitic stainless steels) because it was difficult to obtain SUS304 steel with a 100 % martensite fraction.

Table I lists those J–A parameters together with the obtained values of the martensite fraction, average aspect ratio, most probable orientation angle θ_{mod} , and probability density function parameters P_1 and S_1 for each specimen. The angle θ_{mod} decreases with increasing maximum strain up to a maximum strain of 0.2. For larger maximum strains, θ_{mod} remains constant, but the half-width of $g(\theta, 0)$ decreases.

Fig. 3(a) shows the relationship between the parameter ψ , obtained using Eq. (15) and the permeability versus magnetic field relationship of SUS304 steel calculated using the parameters in Table I and the equations in Section II, and the maximum strain. Fig. 3(b) shows the relationship between the orientation angle θ and the parameters ψ_L and ψ_T (where the L and T subscripts indicate that the magnetic field and permeability are parallel to the x_3 - and x_1 -axis, respectively), calculated

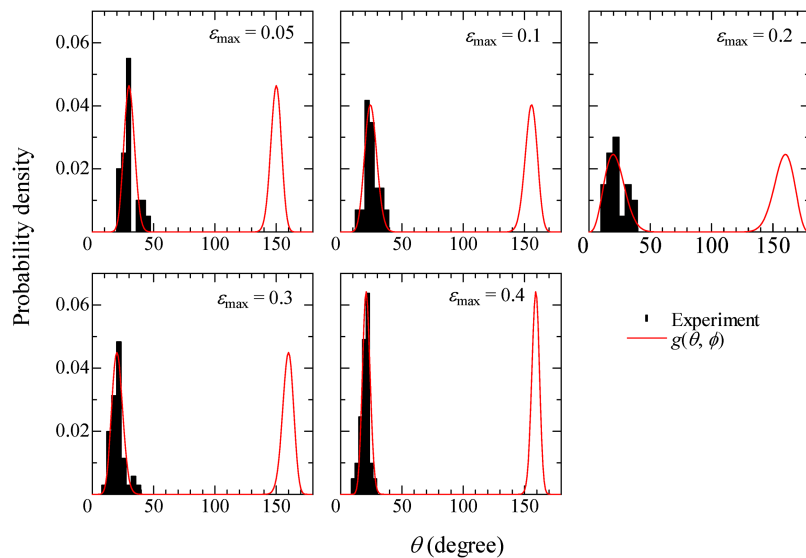


FIG. 2. Histogram and probability density function of the orientation angle of martensite particles, for different values of the maximum strain ε_{max} .

TABLE I. Parameters of the material used in the numerical analysis.

	Maximum strain				
	0.05	0.1	0.2	0.3	0.4
Volume fraction	0.0017	0.0028	0.012	0.033	0.070
Aspect ratio	31	30	41	44	56
θ_{mod} (degrees)	30	24	20	20	21
P_1	12	6	2	5	12
Q_1	165	127	46	159	328
J-A parameter	α	a (A/m) ^a	k (A/m)	c	M_s (MA/m)
	0.0029	1312	457	0.051	1.27

^a a is the parameter of the Langevin function.

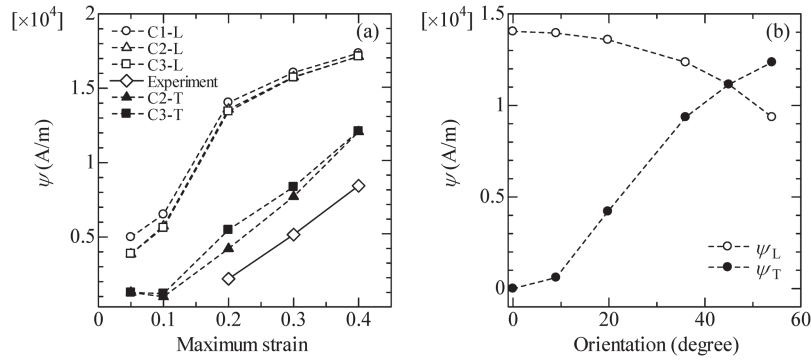


FIG. 3. Relationship between the evaluation parameter ψ of the permeability curve and (a) the maximum strain, (b) the orientation angle for a maximum strain of 0.2. The experimental values in (a) have been multiplied by an additional factor of 10^{-1} .

using the parameter values for a maximum strain of 0.2. C1, C2, and C3 indicate that the analysis was performed using $\theta = 0^\circ$, $\theta = \theta_{\text{mod}}$, and $g(\theta, 0)$, respectively. The experimental values in Fig. 3(a) are multiplied by an additional factor of 10^{-1} with respect to the computed values. The ψ_T value for the case C1 was not plotted because it was negligible. Although the calculated and experimental values are markedly different, the qualitative behavior of ψ_L is quite similar, increasing linearly with maximum strain. The quantitative difference between the experimental and analysis result is a result of estimating the J-A parameters using SUS410S. Obtaining the magnetization curve of a martensite particle is a future challenge. For a maximum strain of 0.05, the ψ_L value in the case C2 is 22% smaller than in the case C1, which clearly shows that the orientation angle has effect on ψ_L . On the contrary, the ψ_L values in the cases C2 and C3 are about the same, even though the half-width of $g(\theta, 0)$ is different; this means that the distribution of orientation angles has little effect on ψ_L . On the other hand, the effect of the orientation distribution on ψ_T is observed clearly for maximum strains of 0.2 and 0.3. In particular, for a maximum strain of 0.2, the ψ_T value in the case C3 is 30% larger than in the case C2. The reason for this can be understood from Fig. 3(b). If we assume that the EMPs are uniformly oriented for $0^\circ < \theta < 40^\circ$, we can consider that the areas under the ψ -curves in Fig. 3(b) are nearly equivalent to those in the case C3. Because ψ_T is nearly zero for $\theta < 10^\circ$, the area under the ψ_T -curve on the interval $20^\circ < \theta < 40^\circ$ is about seven times larger than that on $0^\circ < \theta < 20^\circ$. For a maximum strain of 0.2, $g(\theta, 0)$ is symmetric about $\theta = 20^\circ$ and has large half-width; hence, the ψ_T value in the case C3 receives a significant contribution from angles $20^\circ < \theta < 40^\circ$ and becomes larger than in the case C2. On the other hand, the area under the ψ_L -curve on the interval $20^\circ < \theta < 40^\circ$ is smaller than the area on $0^\circ < \theta < 20^\circ$, but only about 1.1 times. As a result, the ψ_L values in the cases C3 and C2 are very similar, though the C3 value is slightly smaller.

V. CONCLUSION

In this study, we derived a magnetic composite model to account for misoriented martensite particles, and investigated the effects of these particles on the permeability curve. The developed model is able to qualitatively reproduce the change in permeability caused by misoriented martensite particles. We found that the effect of the orientation distribution on the permeability curve depends on the relative orientation between the martensite particles and the magnetic field.

ACKNOWLEDGMENTS

I would like to express my appreciation to Tomimoto Yusuke, a master's student at Kyoto University, for his help in the performance of the experiments. This work was supported by JSPS KAKENHI Grant Number16K06386.

- ¹ A. Das, *J. Mag. Mag. Mater.* **361**, 232 (2014).
- ² H. Li, Z. Chen, Y. Li, T. Takagi, T. Uchimoto, N. Chigusa, and Y. Yoshida, *Int. J. Appl. Elec. Mech.* **38**, 17 (2012).
- ³ V. B. Bregar and M. Pavlin, *J. Appl. Phys.* **95**, 6289 (2004).
- ⁴ P. Quéffélec, D. Bariou, and P. Gelin, *IEEE Trans. Magn.* **41**, 17 (2005).
- ⁵ T. Mura, *Micromechanics of Defects in Solids*, 2nd ed. (Kluwer, Dordrecht, 1991).
- ⁶ J. Y. Li and M. L. Dunn, *J. Intell. Mater. Syst. Struct.* **9**, 404 (1998).
- ⁷ K. Kinoshita, R. Nakazaki, and E. Matsumoto, *Int. J. Appl. Elec. Mech.* **45**, 45 (2014).
- ⁸ R. V. Iyer and P. S. Krishnaprasad, *Nonlinear Anal.-Theor.* **61**, 1447 (2005).
- ⁹ T. Mori and K. Tanaka, *Acta Metall.* **21**, 571 (1973).
- ¹⁰ H. Hatta and M. Taya, *J. Appl. Phys.* **58**, 2478 (1985).
- ¹¹ M. L. Dunn and M. Taya, *Proc. R. Soc. Lond. A* **443**, 265 (1993).
- ¹² M. Taya, *Electric Composites* (Cambridge, University Press, Cambridge, 2008), p.131.
- ¹³ Z. Maekawa, S. Yamada, and H. Mizouchi, *J. Soc. Mater. Sci. Jpn.* **39**, 38 (1990) (in Japanese).
- ¹⁴ H. Hayakawa and M. Nagumo, *Tetsu-to-Hagané* **89**, 289 (2003) (in Japanese).